# Carbon monoxide annealed $TiO_2$ nanotube array electrodes for efficient biosensor applications†

**Yunhuai Zhang,[ab] Peng Xiao,[ac] Xiaoyuan Zhou,[a] Dawei Liu,[a] Betzaida Batalla Garcia[a] and Guozhong Cao*[a]**

*Received 21st October 2008, Accepted 24th November 2008*
*First published as an Advance Article on the web 15th December 2008*
**DOI: 10.1039/b818620k**

Highly ordered titania nanotube (TNT) arrays fabricated by anodic oxidation of titanium foil followed with $O_2$ and CO annealing were employed as matrices for the immobilization of horseradish peroxidase (HRP) and thionine chloride (Th) for biosensor application. The influence of annealing gases on TNT crystallinity, morphology, surface chemistry, and electrochemical properties were investigated by means of X-ray diffraction (XRD), scanning electron microscopy (SEM), photoelectron spectroscopy (XPS), and cyclic voltammetry. The results showed that TNT arrays annealed in CO consisted of $Ti^{3+}$ defects with carbon-doping and exhibited well defined quasi-reversible cyclic voltammetric peaks, indicating enhanced electron transfer and electrical conductivity. When immobilized with HRP and Th, the TNT electrodes were used to sense hydrogen peroxide ($H_2O_2$) as investigated by means of UV-Vis absorption spectroscopy, cyclic voltammetry, and amperometry. The results indicated that the biosensor based on a TNT array electrode annealed in CO possessed greatly enhanced properties compared to the as-grown and the $O_2$-annealed TNT array electrodes. The improved biosensor properties of the $TiO_2$ nanotube arrays were ascribed to the carbon-doping and the formation of $Ti^{3+}$ defects.

## 1. Introduction

Nanostructured $TiO_2$, particularly $TiO_2$ nanotubes (TNT), which possess large surface areas, have been widely used as chemical sensors,[1–3] and catalytic[4–8] and solar cells.[9–11] Due to its nontoxicity, good biocompatibility and environmental safety, TNT have also been explored for immobilizing proteins and enzymes in biomaterial and biosensor applications.[12,13] Recently more research efforts have been devoted to the synthesis, characterization and applications of self-organized $TiO_2$ nanotube arrays with well defined and controlled nanostructures by means of acidic anodization of titanium foils.[14,15] The diameters and lengths of the TNT can be easily tailored by controlling the synthesis parameters of the anodization process. Such ordered $TiO_2$ nanotube arrays offer high surface areas, well defined nanostructures, favorable transport pathways, and good adhesion to the substrate, and have thus become a favorable choice of electrodes for chemical and biosensors, in which the sensitivity is dependent on both surface reaction and charge transfer. $TiO_2$ is a versatile electrode material that can undergo various chemical and physical modifications to produce suitable surface chemistry for the adsorption of organic molecules and biological molecules. It has been reported that surface defects including step edges, oxygen vacancies, line defects, impurities, and crystallographic shear planes have significant effects on the electrocatalytic activity, photocatalytic activity, and sensor properties of the $TiO_2$ nanotubes. Among these defects, oxygen vacancies in conjunction with the conversion of $Ti^{4+}$ to $Ti^{3+}$ can be obtained by ion sputtering,[16] electron beam bombardment,[17] thermal annealing in controlled gas,[18] and low energy ultraviolet photons illumination.[19] Annealing $TiO_2$ in various conditions can effectively alter the crystal structure and defect concentration.[20–23] Surface defects can have an appreciable influence on adhesion and sorption properties. For example, by annealing in vacuum at low temperature, Guillemot *et al.*[24] enhanced the $Ti^{3+}$ defects density in Ti-6Al-4V alloys and improved bone–implant interactions. In addition, doping with nitrogen, carbon, and boron has been reported as another way to enhance the electrocatalytic and photocatalytic activity of $TiO_2$.[25–27]

For electrochemical enzyme biosensors, the electrodes need to meet a number of important criteria including: (a) high electrochemical activity, (b) high enzyme loading capacity, and (c) fast sorption and reaction kinetics. As highly ordered $TiO_2$ nanotube arrays offer high surface area, favorable transport pathways, and good electrochemical properties; they are a favorable choice of electrodes as supporting matrices for biosensors. However, without annealing, the electrochemical and biosensor performance of the as-grown TNT array was unsatisfactory due to its poor electrical conductivity.[13] When annealed in dry nitrogen, air, and argon at various temperatures, TNT arrays demonstrated appreciably different electrochemical properties. For example, TNT array annealed in nitrogen demonstrated much improved electrochemical properties as compared to that of as-grown TNT arrays, annealed in air or argon.[28]

In this work, we demonstrate a greatly improved biosensor based on $TiO_2$ nanotube arrays annealed in CO, which resulted

[a]*Department of Materials Science and Engineering, University of Washington, Seattle, WA, USA. E-mail: gzcao@u.washington.edu; Fax: +01 2065433100; Tel: +01 2066169084*
[b]*College of Chemical Engineering, Chongqing University, Chongqing, P.R. China*
[c]*Department of Physics, Chongqing University, Chongqing, P.R. China*
† This paper is part of a *Journal of Materials Chemistry* theme issue on Nanotubes and Nanowires. Guest editor: Z. L. Wang.

 

in carbon-doping and the formation of trivalent titanium ions. Both carbon doping and cationic defects not only improve the electron transfer properties, but also modify the surface chemistry favoring the adsorption of enzymes, leading to greatly improved biosensor performance. Fig. 1 shows a schematic representation of a highly ordered TNT array biosensor co-adsorbed with HRP and Th. The TNT arrays were synthesized by anodizing titanium foil. After annealing in CO, HRP and Th were co-immobilized on the TNT arrays and the electrodes were employed to detect hydrogen peroxide. The influence of annealing gases on the defects and surface chemistry of TNT arrays was studied by means of XPS, XRD and SEM. The influence of surface defects and carbon-doping on the biosensor properties of $TiO_2$ nanotube arrays were investigated and discussed.

## 2. Experimental

Titanium foil (99% pure, 0.5 mm thick), potassium fluoride (KF, 99%) and sodium hydrogen sulfate ($NaHSO_4$, 98%) were purchased from VWR. The growth of titania nanotube arrays by anodization has been reported widely in the literature and the growth conditions used in this work are similar to those reported in our earlier publications[13] and are briefly reiterated below. The titanium foils were ultrasonically cleaned in 18% HCl solution, followed by rinsing with deionized water, and ultrasonic rinsing in acetone prior to acidic anodization. The electrolyte was composed of 0.1 M KF, and 1.0 M $NaHSO_4$, sodium hydroxide solution was added to adjust the pH value to 3.5–4.5 as measured with a pH meter (Model 3000, VWR scientific). The anodization was conducted in a two-electrode cell with a platinum foil as the cathode, approximately 2 cm apart from the Ti anode, and a constant applied voltage of 20 V. The anodization time was 1 h. The resultant TNT arrays were thoroughly rinsed with deionized water. The TNT arrays were annealed at 500 °C in a tube furnace, under a flow of dry $O_2$ and CO, respectively, with a heating rate of 5 °C $min^{-1}$ and a dwelling time of 3 h.

The annealed TNT arrays were first sealed with epoxy resin leaving an open area of 0.5 $cm^2$, then immersed in 3 ml of 5 mM phosphate buffer (PB) solution at pH 7.0 containing 1.8 mg thionine chloride (Th) and 3.6 mg horseradish peroxide (HRP) for 24 hours to produce Th/HRP-modified electrodes. The resultant electrodes were stored in 5 mM PB of pH 7.0 at 4 °C.

The carbon-doping and $Ti^{3+}$ defect concentrations were measured by means of X-ray photoelectron spectroscopy (XPS, SSL-300 system, C1s was used as reference to calibrate the peaks). The surface morphology of the $TiO_2$ nanotubes before and after annealing was characterized by scanning electron microscopy (SEM, Philips, JEOL JSM7000). UV-Vis absorption spectra were measured using a DU72 UV-Vis Spectrometer. The electrochemical properties of the TNT electrodes were monitored in 1 M KCl solution at 0.1 V $s^{-1}$ in the presence of 10 mM $K_3[Fe(CN)_6]$ using an electrochemical workstation (CHI 605C), which was also used to investigate the biosensor response to $H_2O_2$, where Pt foil and Ag/AgCl electrode were used as the counter electrode and reference electrode respectively.

## 3. Results and discussion

### 3.1 Structural characterization of TNT arrays

Fig. 2 shows SEM images of TNT arrays (A) before annealing, (B) after annealing in $O_2$ at 500 °C for 3 h, and (C) after annealing in CO at 500 °C for 3 h. The average diameter and wall thickness of TNT were estimated from the SEM images and averaged over a large area. The as-grown TNT have an inner diameter of ~90 nm, wall thickness of ~8 nm, and tube length of ~1.5 μm. After annealing at 500 °C in $O_2$ and CO for 3 h, the inner diameter decreased to ~85 nm, the wall thickness increased to 15 nm, and the tube length decreased to ~1.3 μm. As expected, the increase of wall thickness was accompanied by a decrease in

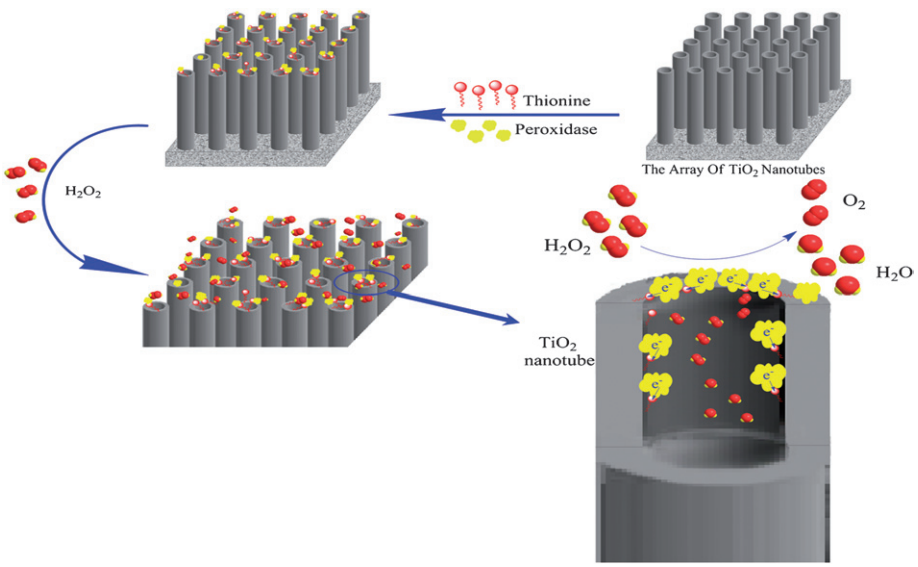


**Fig. 1** Schematic representation of highly ordered $TiO_2$ nanotube array biosensor showing the co-immobilization of enzymes and the sensing mechanism.

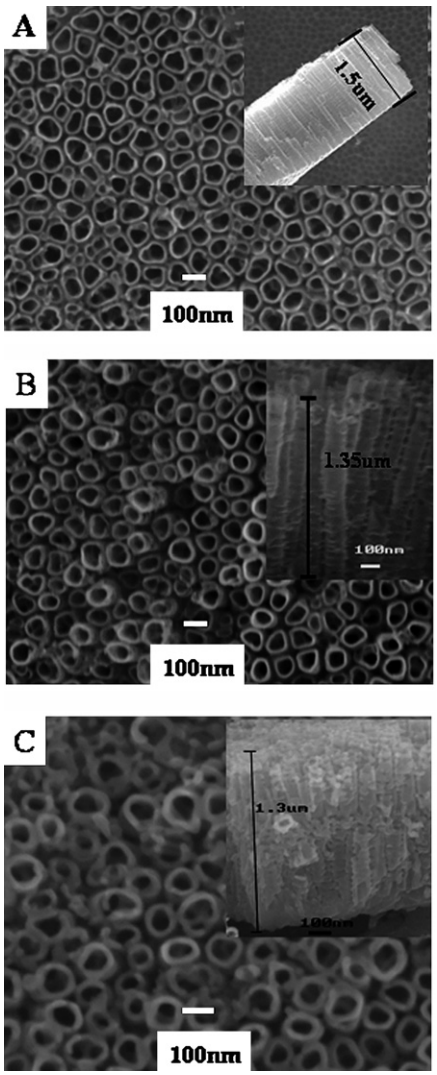


**Fig. 2** SEM images of the cross-section and top-surface morphology (inset) of (A) an as-grown TNT array without annealing, (B) a TNT array annealed in $O_2$ at 500 °C, and (C) a TNT array annealed in CO at 500 °C.

the length of TNT according to SEM cross-section images. Such a change of morphology is ascribed to partial sintering and has been described in the literature.[29] It is noted that annealing at 500 °C in CO for 3 h resulted in the formation of some holes in the TNT wall surface. However, when annealed in $O_2$, TNT morphology is more stable at 500 °C as indicated in Fig. 2.

Fig. 3 compares the XRD patterns of TNT arrays annealed in $O_2$ and CO for 3 h at 500 °C. It can be seen that the anatase phase of $TiO_2$ is the main crystalline phase in both samples annealed at 500 °C. However, the rutile phase was detected in the TNT array annealed in CO at 500 °C, while no rutile phase was present in the TNT array annealed in $O_2$. The relatively easy phase transition from anatase to rutile at 500 °C in CO gas compared to $O_2$ gas could possibly be ascribed to easier nucleation at the surface promoted by the surface defects that result from annealing in CO, which will be discussed further in the following section. Using the Scherrer equation, the crystallite size of anatase titania was estimated to be ~17 nm for the TNT array annealed in $O_2$ and ~14 nm for the TNT array annealed in CO. The smaller

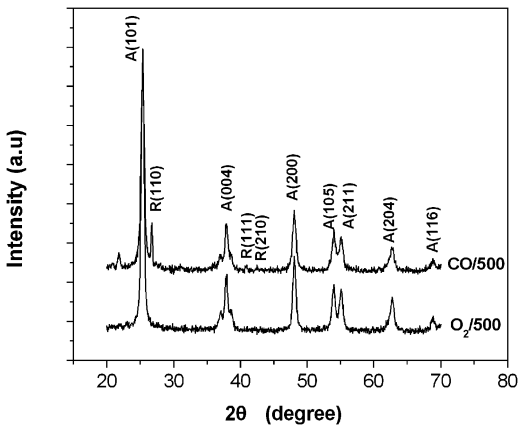


**Fig. 3** The XRD patterns of TNT array annealed in a flow of $O_2$ and in CO gases at 500 °C for 3 h: only the anatase phase was identified in the TNT arrays annealed in oxygen, while a small fraction of rutile phase was detected in the TNT array annealed in CO.

grain size in CO-annealed TNT array may also be attributed to possible surface defects that may restrict the grain growth. The seemingly contradictory grain size and wall thickness may be due to the different methods used for the estimation; however, it is most likely that the $TiO_2$ nanotubes are made of monolayer of $TiO_2$ nanocrystals.

### 3.2 Carbon-doping and formation of $Ti^{3+}$ defects on $TiO_2$ nanotube surface

Fig. 4A is the C1s XPS spectra of TNT arrays annealed in CO and $O_2$ gas at 500 °C. The C1s spectra revealed three peaks positioned at 289.0 eV, 285.1 eV and 281.7 eV for TNT array annealed in CO (Fig. 4A(a)), but two peaks (289.0 eV and 285.1 eV) in TNT arrays annealed in $O_2$ (Fig. 4A(b)). The peak position of 285.1 eV is close to the position of graphitic $sp^2$ hybridized carbon (284.97 eV) as reported by Gu *et al.*[30] and the peak at 289.0 eV could be assigned to C/O groups resulting from the absorption of $CO_2$ and CO onto the surface of TNT. The peak at 281.7 eV in the TNT arrays annealed in CO could possibly be ascribed to TiC, suggesting possible carbon doping as reported in the literature.[4]

From the Ti–C peak intensity, the doping concentration of carbon is estimated to be ~2.4% in TNT arrays annealed in CO at 500 °C for 3 h using the method reported by Park *et al.*[4] However, Park *et al.* obtained the carbon concentrations based on C–C peak intensity, as they could not find significant signals from carbide (Ti–C, 281.5 eV).[4] Fig. 4(B) shows the Ti2p spectra of TNT arrays annealed in CO and $O_2$ at 500 °C for 3 h. In addition to two characteristic peaks of $Ti2p_{1/2}$ at ~465 eV, and $Ti2p_{3/2}$ at ~459 eV,[31] there were two extra peaks at 456.8 eV and 454.9 eV found in the TNT array annealed in CO (spectrum a), but not in the TNT arrays annealed in $O_2$ (spectrum b). According to the literature,[14,32,33] these two peaks are assigned to $Ti^{3+}$ at ~456.8 eV and Ti–C at 454.9 eV, though there were energy shifts in the peak positions for $Ti^{3+}$ (2.0 eV) and TiC (3.9 eV). Both C1s and Ti2p XPS spectra strongly suggested that CO annealing likely resulted in the introduction of carbon to the

 

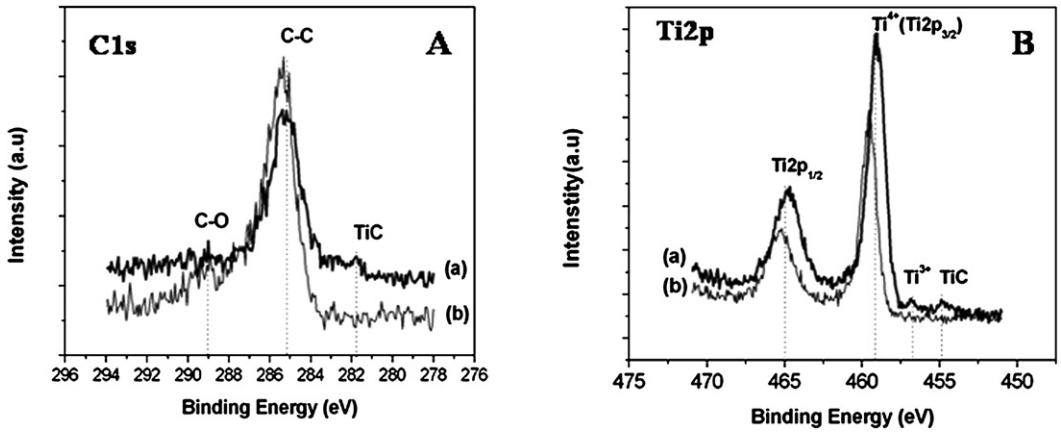


**Fig. 4** C1s and Ti2p XPS spectra of TNT annealed in CO and $O_2$ at different temperatures. (A) C1s XPS spectra of samples annealed in CO at 500 °C (a) and in $O_2$ at 500 °C (b). (B) T2p XPS spectra of samples annealed in CO at 500 °C (a) and in $O_2$ at 500 °C (b).

crystal structure of $TiO_2$ and the formation of trivalent titanium cations, at least on the surface of TNT arrays.

### 3.3 Electrochemical characteristics

The electrochemical properties of TNT array electrodes annealed in CO and $O_2$ were investigated by means of cyclic voltammetry with 10 mM $K_3[Fe(CN)_6]$ as an electrolyte at a sweep rate of 0.1 V $s^{-1}$. Fig. 5 shows the CV curves for TNT array electrodes annealed in $O_2$ and CO at 500 °C for 3 hours. $O_2$-annealed TNT array electrodes had an oxidation peak at 1.0 V and reduction peak at −0.38 V. The gap between reduction and oxidation peaks was approximately 1.38 V. This large peak separation was assumed to result from the low electrical conductivity of the $TiO_2$ nanotube array electrodes. CO-annealed TNT array electrodes exhibited a pair of well defined oxidation/reduction peaks centered at 0.36 V and 0.19 V, and a gap between the peaks of merely 0.17 V, indicating a quasi-reversible electrochemical reaction of $K_3[Fe(CN)_6]$. The peak gap in CO-annealed TNT array electrodes was less than 13% of the gap in $O_2$ TNT array electrode, suggesting a greatly enhanced electrical conductivity. In addition, the peak current of 1.52 mA, was more than one order of magnitude higher than that of $O_2$-annealed TNT array electrode (<0.1 mA). The greatly enhanced electrical conductivity in CO-annealed TNT array electrodes could be attributed to the presence of trivalent titanium cations and carbon doping, which also serves as indirect evidence of carbon doping and formation of trivalent titanium cations in TNT arrays when annealed in CO, but not in $O_2$-annealed TNT array electrodes.

### 3.4 The adsorption of HRP and Th on TNT arrays

Fig. 6 shows the UV-Vis absorption spectra of (a) the as-prepared HRP and Th solution, (b) the solution after HRP and Th were partially adsorbed onto as-grown TNT arrays, (c) the solution after HRP and Th were partially adsorbed onto TNT arrays annealed in $O_2$, and (d) the solution after HRP and Th were adsorbed onto TNT arrays annealed in CO at 500 °C for 24 h.

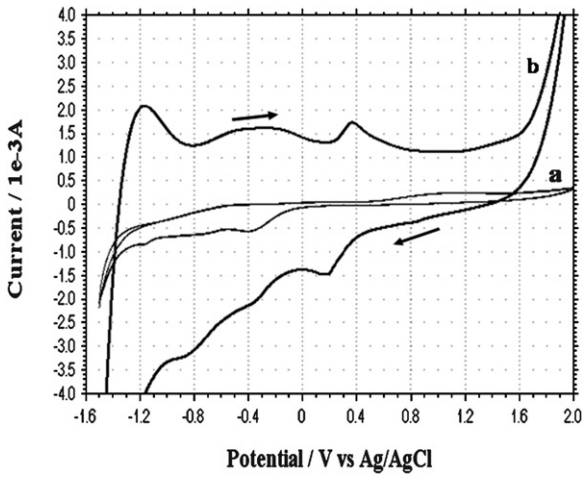


**Fig. 5** Typical CV curves for (a) a TNT array electrode annealed in $O_2$ at 500 °C and (b) a TNT array electrode annealed in CO. The measurements were taken in 1 M KCl solution at 0.1 V $s^{-1}$ in the presence of 10 mM $K_3[Fe(CN)_6]$.

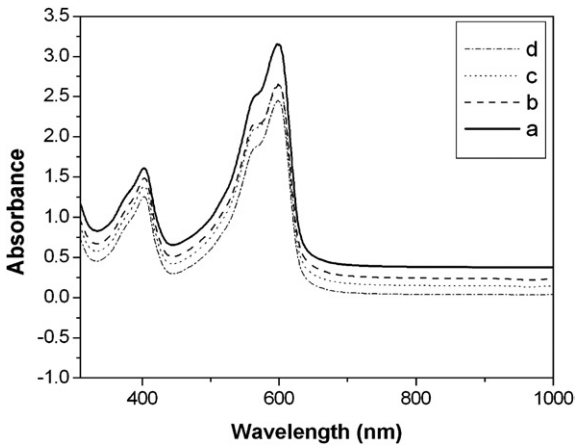


**Fig. 6** The UV-Vis absorbance spectra of (a) the as-prepared solution (1.8 mg Th and 3.6 mg HRP in 3 ml of 5 mM PB) and the solution after HRP and Th were partially adsorbed onto (b) as-grown TNT arrays, (c) TNT arrays annealed in $O_2$, and (d) TNT arrays annealed in CO at 500 °C for 24 h.

The characteristic absorption peaks of HRP at 403 nm and Th at 599 nm were both appreciably reduced in spectra b, c, and d, indicating both HRP and Th were removed from the solution and immobilized on the TNT array electrodes. The amounts of HRP and Th adsorbed were estimated from the change of peak intensities at 403 nm and 599 nm, respectively. Table 1 summarizes the amount of HRP and Th adsorbed on various TNT array electrodes, and it was found that the amounts of HRP and Th adsorbed on TNT were strongly affected by annealing conditions.

The amounts of HRP adsorbed onto TNT array electrodes increased from 0.069 mg (3.25 μg $cm^{-2}$) on as-grown TNT arrays, to 0.071 mg (3.94 μg $cm^{-2}$) on $O_2$-annealed TNT arrays, to 0.159 mg (9.14 μg $cm^{-2}$) on CO-annealed TNT arrays. TNT array annealed in CO at 500 °C adsorbed the highest surface concentration of HRP, almost 3 times that adsorbed on as-grown and $O_2$-annealed TNT arrays. Similarly, the amount of Th adsorbed to TNT array electrodes demonstrated the same increasing trend, though it was less significant. Nevertheless, the amount of Th adsorbed on CO-annealed TNT arrays was approximately 50% higher than that on as-grown TNT arrays, and 30% higher than that on $O_2$-annealed TNT arrays. Although the exact mechanism of such enhanced HRP and Th adsorption is not clear, the surface defects and carbon doping in CO-annealed TNT array are likely to be the factors causing such a change.

### 3.5 The response of $TiO_2$ nanotube array biosensors to hydrogen peroxide

Fig. 7 shows the typical CV curves of as-grown, $O_2$ and CO-annealed TNT array electrodes co-immobilized with both HRP and Th in 0.1 M PB at pH 7.0 in the presence of 5 mM $H_2O_2$ at a scan rate of 100 mV $s^{-1}$. A drastic increase in the reduction current was observed for TNT/CO (curve c) compared with as-grown and $O_2$-annealed TNT array electrodes. The response mechanism of the electrode to $H_2O_2$ can be described by the following reactions:

$$\mathrm{HRP(red)} + \mathrm{H_2O_2} \rightarrow \mathrm{HRP(ox)} + \mathrm{H_2O} \quad (1)$$

$$\mathrm{HRP(ox)} + \mathrm{Th(red)} \rightarrow \mathrm{HRP(red)} + \mathrm{Th(ox)} \quad (2)$$

$$\mathrm{Th(ox)} + 2\mathrm{H^+} + 2\mathrm{e^-} \rightarrow \mathrm{Th(red)} \quad (3)$$

where the immobilized HRP(red) initially reduces $H_2O_2$ to form water and HRP(ox), followed by the oxidation of Th(red) to form HRP(red) and Th(ox) and the reduction of Th(ox) to form Th(red), resulting in an increase in reduction current at about −0.36 V in the CV curve.

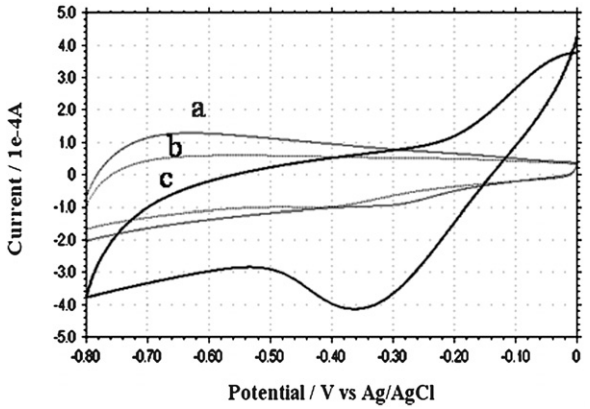


**Fig. 7** Typical CV curves for the response of HRP/Th immobilized TNT array biosensors to $H_2O_2$ for (a) an as-grown TNT array electrode, (b) an $O_2$-annealed TNT array electrode, (c) a CO-annealed TNT array electrode. The measurements were performed in 0.1 M PB at pH 7.0 in the presence of 5 mM $H_2O_2$ at a scan rate of 100 m V $s^{-1}$.

Fig. 8A shows the typical amperometric response of (a) as-grown TNT/HRP/Th, (b) TNT/$O_2$/HRP/Th, and (c) TNT/CO/HRP/Th biosensors to $H_2O_2$ respectively, under the optimized experimental conditions. It was noted that the stable amperometric response could be observed at −0.36 V with successive additions of $H_2O_2$ into 0.1 M PB solution at pH 7.0. Fig. 8B shows the reduction current as function of the $H_2O_2$ concentration. The reduction current for 2.0 mM $H_2O_2$ was 38.2 μA for the as-grown TNT/HRP/Th electrode, 56.0 μA for the TNT/$O_2$/500/HRP/Th electrode and 344.0 μA for TNT/CO/500/HRP/Th electrode. At the $H_2O_2$ concentration of 10 mM, the difference in reduction current is approximately an order of magnitude (∼1000 μA in CO-annealed TNT array biosensors *versus* <100 μA in both as-grown and $O_2$-annealed TNT array biosensors). Obviously the CO-annealed TNT array biosensor possesses significantly higher sensitivity than both as-grown and $O_2$-annealed TNT array biosensors. Such significant enhancement in sensitivity in CO-annealed TNT array biosensors could be attributed to both enhanced electrical conductivity and efficient adsorption of both HRP and Th enzymes. In particular, the significantly increased amount of HRP adsorbed onto the surface of CO-annealed TNT array electrode is more likely to result in a noticeable enhancement of the sensitivity, as the oxidation of HRP (reaction (1)) is likely to be the rate-limiting process.[13] Furthermore, it was found that the TNT/CO/HRP/Th biosensor retains 85% of its initial current response after storing for one week in 0.1 M PB solution in the refrigerator at 4 °C, showing an acceptable shelf life.

**Table 1** The structure and the absorbance of HRP and Th on different TNT electrodes[a]

| | ID/nm | WT/nm | Length/μm | Surface area/($cm^2$/$cm^2$) | A1 | A2 | A3 | A4 |
|---|---|---|---|---|---|---|---|---|
| As-grown TNT | 90 | 8 | 1.50 | 42.4 | 0.069 | 3.25 | 0.251 | 11.85 |
| TNT/$O_2$/500 | 86 | 14 | 1.35 | 36.0 | 0.071 | 3.94 | 0.240 | 13.35 |
| TNT/CO/500 | 85 | 15 | 1.30 | 34.7 | 0.159 | 9.14 | 0.305 | 17.56 |

[a] ID: internal diameter of TNT; WT: wall thickness; A1: the amount of HRP adsorbed (mg); A2: the amount of HRP adsorbed per surface area (μg $cm^{-2}$); A3: the amount of Th adsorbed (mg); A4: the amount of Th adsorbed per surface area (μg $cm^{-2}$).

 

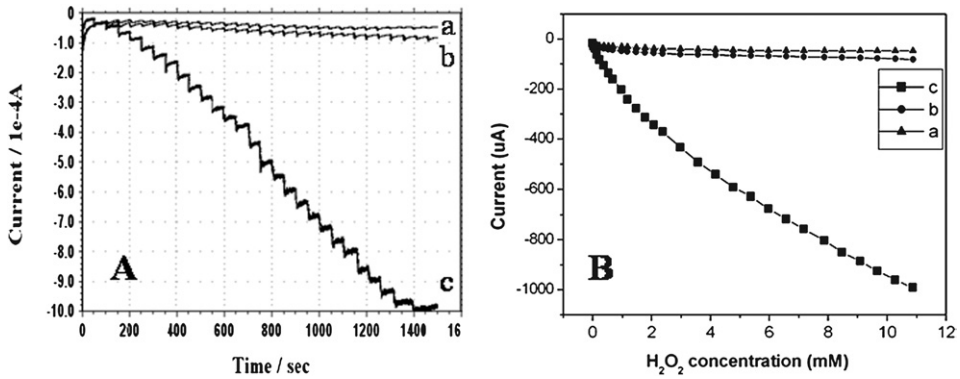


**Fig. 8** A) The amperometric response of TNT biosensors to successive additions of 50 mM $H_2O_2$ solution for (a) as-grown TNT/HRP/Th, (b) TNT/$O_2$/HRP/Th and (c) TNT/CO/HRP/Th. B) Calibration curves for (a) as-grown TNT/HRP/Th, (b) TNT/$O_2$/HRP/Th, and (c) TNT/CO/HRP/Th biosensors.

## 4. Conclusions

This study demonstrated that annealing in CO at 500 °C is mostly likely to have resulted in the formation of trivalent titanium ions and carbon doping, at least on the surface of titania nanotube arrays fabricated by acidic anodization of titanium foil, as compared to the as-grown and $O_2$-annealed TNT arrays. The presence of trivalent titanium ions and carbon dopants appreciably enhanced the electrochemical properties and modified the surface chemistry of the CO-annealed TNT arrays, leading to very efficient adsorption of HRP and Th. The amount of HRP adsorbed on CO-annealed TNT arrays was three times the amount adsorbed on as-grown or $O_2$-annealed TNT arrays. Better electrical conductivity and a high density of HRP were believed to be responsible for the much improved biosensor sensitivity of CO-annealed TNT array biosensors.

## Acknowledgements

YHZ and PX gratefully acknowledge the fellowship from the Chinese Scholarship Council and the support of Science Foundation of Chongqing Science and Technology Committee (CSTS, 2007BB4157), DWL wants to acknowledge the graduate fellowship from the Center for Nanotechnology at the University of Washington, and BBG gratefully acknowledges traineeship support provided by the University of Washington Bioenergy IGERT (DGE-0654252). This work was supported in part by National Science Foundation (DMI-0455994) and Air Force Office of Scientific Research (AFOSR-MURI, FA9550-06-1-032).

## References

1 Y. B. Xie, L. M. Zhou and H. T. Huang, *Biosens. Bioelectron.*, 2007, **22**, 2812–2818.
2 D. V. Bavykin, E. V. Milsom, F. Marken, D. H. Kim, D. H. Marsh, D. J. Riley, F. C. Walsh, K. H. El-Abiary and A. A. Lapkin, *Electrochem. Commun.*, 2005, **7**, 1050–1058.
3 H. Tsuchiya, J. M. Macak, L. Muller, J. Kunze, F. Muller, P. Greil, S. Virtanen and P. Schmuki, *J. Biomed. Mater. Res., Part A*, 2006, **77A**, 534–541.
4 J. H. Park, S. Kim and A. J. Bard, *Nano Lett.*, 2006, **6**, 24–28.
5 X. Quan, S. G. Yang, X. L. Ruan and H. M. Zhao, *Environ. Sci. Technol.*, 2005, **39**, 3770–3775.
6 G. K. Mor, K. Shankar, M. Paulose, O. K. Varghese and C. A. Grimes, *Nano Lett.*, 2005, **5**, 191–195.
7 S. G. Yang, Y. Z. Liu and C. Sun, *Appl. Catal., A*, 2006, **301**, 284–291.
8 S. P. Albu, A. Ghicov, J. M. Macak, R. Hahn and P. Schmuki, *Nano Lett.*, 2007, **7**, 1286–1289.
9 O. K. Varghese and C. A. Grimes, *Sol. Energy Mater. Sol. Cells*, 2008, **92**, 374–384.
10 K. G. Ong, O. K. Varghese, G. K. Mor, K. Shankar and C. A. Grimes, *Sol. Energy Mater. Sol. Cells*, 2007, **91**, 250–257.
11 M. S. Akhtar, J. M. Chun and O. B. Yang, *Electrochem. Commun.*, 2007, **9**, 2833–2837.
12 J. M. Macak, H. Tsuchiya, L. Taveira, A. Ghicov and P. Schmuki, *J. Biomed. Mater. Res., Part A*, 2005, **75**, 928–933.
13 P. Xiao, B. B. Garcia, Q. Guo, D. W. Liu and G. Z. Cao, *Electrochem. Commun.*, 2007, **9**, 2441–2447.
14 J. M. Macak, H. Tsuchiya and P. Schmuki, *Angew. Chem., Int. Ed.*, 2005, **44**, 2100–2102.
15 S. P. Albu, A. Ghicov, J. M. Macak and P. Schmuki, *Physica Status Solidi RRL.*, 2007, **1**, R65–R67.
16 S. Petigny, H. Mostefa-Sba, B. Domenichini, E. Lesniewska, A. Steinbrunn and S. Bourgeois, *Surf. Sci.*, 1998, **410**, 250–257.
17 L. Q. Wang, D. R. Baer and M. H. Engelhard, *Surf. Sci.*, 1994, **320**, 295–306.
18 H. Norenberg, F. Dinelli and G. A. D. Briggs, *Surf. Sci.*, 2000, **446**, L83–L88.
19 R. Wang, K. Hashimoto, A. Fujishima, M. Chikuni, E. Kojima, A. Kitamura, M. Shimohigoshi and T. Watanabe, *Nature*, 1997, **388**, 431–432.
20 K. Noworyta and J. Augustynski, *Electrochem. Solid-State Lett.*, 2004, **7**, E31–E33.
21 G. K. Mor, O. K. Varghese, M. Paulose, K. Shankar and C. A. Grimes, *Sol. Energy Mater. Sol. Cells*, 2006, **90**, 2011–2075.
22 A. Ghicov, J. M. Macak, H. Tsuchiya, J. Kunze, V. Haeublein, L. Frey and P. Schmuki, *Nano Lett.*, 2006, **6**, 1080–1082.
23 R. P. Vitiello, J. M. Macak, A. Ghicov, H. Tsuchiya, L. F. P. Dick and P. Schmuki, *Electrochem. Commun.*, 2006, **8**, 544–548.
24 F. Guillemot, M. C. Porte, C. Labrugere and C. Baquey, *J. Colloid Interface Sci.*, 2002, **255**, 75–78.
25 X. M. Fang, Z. G. Zhang, Q. L. Chen, H. B. Ji and X. N. Gao, *J. Solid State Chem.*, 2007, **180**, 1325–1332.
26 N. Lu, X. Quan, J. Y. Li, S. Chen, H. T. Yu and G. H. Chen, *J. Phys. Chem. C*, 2007, **111**, 11836–11842.
27 L. H. Zhang and R. V. Koka, *Mater. Chem. Phys.*, 1998, **57**, 23–32.
28 P. Xiao, D. W. Liu, B. B. Garcia, S. Sepehri, Y. H. Zhang and G. Z. Cao, *Sens. Actuators, B*, 2008, **134**, 367–372.
29 A. Ghicov, H. Tsuchiya, R. Hahn, J. M. Macak, A. G. Munoz and P. Schmuki, *Electrochem. Commun.*, 2006, **8**, 528–532.
30 Y. L. Gu, L. Y. Chen, Y. T. Qian, W. Q. Zhang and J. H. Ma, *J. Am. Ceram. Soc.*, 2005, **88**, 225–227.
31 W. Gopel, J. A. Anderson, D. Frankel, M. Jaehnig, K. Phillips, J. A. Schafer and G. Rocker, *Surf. Sci.*, 1984, **139**, 333–346.
32 L. I. Johansson, *Surf. Sci. Rep.*, 1995, **21**, 179–250.
33 J. Zhao, E. G. Garza, K. Lam and C. M. Jones, *Appl. Surf. Sci.*, 2000, **158**, 246–251.